Asian Journal of Chemistry; Vol. 33, No. 7 (2021), 1638-1644

ASIAN JOURNAL OF CHEMISTRY

https://doi.org/10.14233/ajchem.2021.23259

Crystal Structure, Experimental and DFT of (*Z*)-4-((4-Fluorophenyl)amino)pent-3-en-2-one

P. Jeeva[1], D. Barathi[1,*], K. Prabakaran[2], M. Seenivasa Perumal[3], Ahmet Atac[4] and Etem Kose[4,5]

[1]PG and Research Department of Physics, N.K.R. Government Arts College for Women, Namakkal-637001, India
[2]Department of Advanced Organic Materials Science and Engineering, College of Engineering, Eng. Building # W3, Room No. 238, Chungnam National University, 220 Gung-dong, Yuseong-gu, Daejeon 305-764, Republic of South Korea
[3]Department of Chemistry, Gandhigram Rural Institute (Deemed to be University), Gandhigram-624302, India
[4]Department of Electronic and Automation, Manisa Technical Sciences Vocational School, Manisa Celal Bayar University, TR, 45140, Manisa, Turkey
[5]Department of Physics, Faculty of Art and Sciences, Manisa Celal Bayar University, TR-145140, Manisa, Turkey

*Corresponding author: E-mail: barathi.rammohan@gmail.com

Received: 22 April 2021; *Accepted*: 22 May 2021; *Published online*: 26 June 2021; AJC-20407

Single crystals of a organic compound, (*Z*)-4-((4-fluorophenyl)amino)pent-3-en-2-one (4FPA) were grown by the slow evaporation technique and characterized by X-ray diffraction and FT-IR spectra. The normal mode frequencies, intensities and the corresponding vibrational assignments were calculated using the GAUSSIAN 09W set of quantum chemistry codes at the DFT/B3LYP levels of theory using the 6-31+G(d,p) basis set. The Fourier transform infrared spectrum was obtained for the title molecule at room temperature. Reactivity features were determined based on global descriptors, electron density mapping and Fukui analysis to reveal the electrophilic and nucleophilic coordination of them. The thermodynamic and intramolecular interactions were also investigated. The non-covalent interaction mapped by reduced density gradient method reveals possible methyl (CH_3) influence on the ring and NH groups with their reactivity and non-linear optical properties of 4FPA were found by first-order hyperpolarizability.

Keywords: Density functional theory, NBO, Fukui analysis, Electron density mapping, Non-covalent interaction.

INTRODUCTION

Enaminones possibly act as electrophiles and nucleophiles due to the fact that they have got conjugated the N-C=C-C=O with carbon centers, an electron-rich carbon atom and an amino group [1]. Enaminones are formed by a reaction between a primary amine and a β-dicarbonyl compound. They have been used as intermediates or building blocks in synthetic and medicinal chemistry but they also have biological activities [2] such as antibacterial [3], anti-inflammatory [4], anticonvulsant [5] and antitumour agents [6]. The versatility of enaminones is in great part due to their promptness to both electrophilic and nucleophilic attack [7,8].

Strong solvent effects on the non-linear optical properties (NLO) of *Z*- and *E*-isomers from azo-enaminone derivatives have been reported [9-11]. Crystal structure and quantum chemical studies of a novel push-pull enaminone: 3-chloro-4-((4-bromophenyl)amino)pent-3-en-2-one have been identified [12]. The conformational analysis of push-pull enaminones have reported by Vdovenko *et al*. [13]. Enaminones are optimized using DFT [14]. In present study, (*Z*)-4-((4-fluorophenyl)amino)pent-3-en-2-one (4FPA) was crystallized and subjected to SXRD, FT-IR and thermodynamic properties to investigate its physical and chemical properties [15-17]. Reactivity features were determined based on global descriptors, molecular electrostatic potential (MEP), electron density mapping and Fukui analysis to reveal the electrophilic and nucleophilic nature of molecule. Besides, thermodynamic properties (heat capacity, entropy and enthalpy), non-covalent interactions mapped by the reduced density gradient method. At last NLO of 4FPA was also calculated.

EXPERIMENTAL

Crystal growth of (*Z*)-4-((4-fluorophenyl)amino)pent-3-en-2-one (4FPA): The title crystals were obtained by reacting pentane-2,4-dione (2 mmol), 4-fluoroaniline (2 mmol) in

ethanol (5 mL) and 0.0034 N of onion extract (0.01 mL) at room temperature and stirred for 5 h. Then water and ethyl acetate were added in the above resulting solution. This was extracted using ethyl acetate (2 × 10 mL) and the combined organic extract was washed with water, brine and finally dried with anhydrous Na_2SO_4. Good quality of 4FPA crystals were harvested after slow evaporation of solvent.

Physico-chemical characterization of 4FPA crystals: The lattice parameters and space group of the grown crystal was determined using single crystal XRD analysis. The FT-IR spectrum was recorded using a Perkin-Elmer spectrometer at KBr phase in the vicinity of 4000-400 cm^{-1} with a resolution of 1 cm^{-1}. The UV-VIS optical transmittance spectrum was obtained by JASCO spectrophotometer in the range of 200-800 nm.

Computational details: The structural parameters and vibrational frequencies of the title compound were accomplished with Gaussian 09W software package [18] using the B3LYP/6-31+G (d,p). The vibrational modes were allocated based on the possible distribution of energy using the VEDA4 programme [19]. The photo-physical properties were analyzed *via* Frontier Molecular Orbitals. Furthermore, Multiwfn_3.3.8 [20] and VMD [21] programs were used to obtain the non-covalent interactions (RDG), reactive sites on the molecular surfaces with Fukui function analysis [22], respectively.

RESULTS AND DISCUSSION

Single-crystal XRD analysis: The lattice parameters and space group of 4FPA single crystal are given in Table-1. The crystal belongs to the triclinic system with space group *P*1. The oxygen atom (O1) of the carbonyl group act as acceptor of the hydrogen atoms from the ethylene bridge and phenyl rings.

TABLE-1
CRYSTAL DATA AND STRUCTURE REFINEMENT OF 4FPA SINGLE CRYSTAL

Empirical formula	$C_{11}H_{12}NOF$
Formula weight	193.22
Temperature	294(2) K
Wavelength	0.71073 A
Crystal system, space group	Triclinic, P-1
Unit cell dimensions	a = 9.312(8) Å, α = 111.643(18)°
	b = 10.857(7) Å, β = 97.14(2)°
	c = 12.431(10) Å, γ = 108.561(19)°
Volume	1064.9(15) A^3
Z, Calculated density	4, 1.205 Mg/m^3
Absorption coefficient	0.089 mm^{-1}
Crystal size	0.200 × 0.150 × 0.100 mm

Geometric parameters: The molecular structure of 4FPA molecule was optimized using the DFT/B3LYP/6-31+G(d,p) and is shown in Fig. 1. After optimization, the total energy of the molecule was -656.25 Hartrees. Theoretically calculated geometry values are well agreement with the experimentally determined values. The amine group N3-H15 pushes and the carbonyl O2-C10 pulls electron density through a C8=C9. Due to this, the push-pull effect of amine and carbonyl group through ethylene, the bond length of N3-H15=1.0099 Å is short and

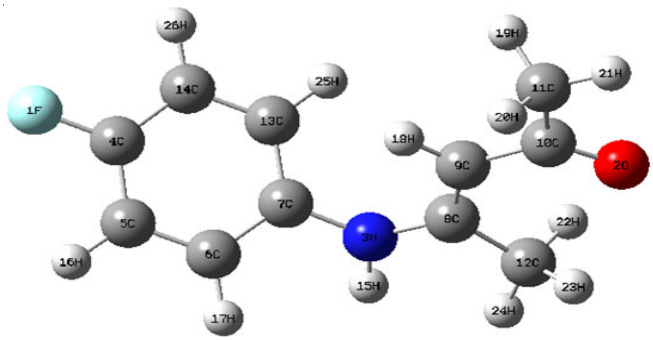

Fig. 1. Optimized geometry of the 4FPA crystals with DFT/B3LYP/6-31+G (d,p)

the bond length of O2-C10=1.2357 Å is long. The C8-C12 and C10-C11 has high bond length among the others due to the possible consequence of π-delocalization around methyl groups [23].

Vibrational (FTIR) investigation: The experimental and theoretical vibrational frequencies for 4FPA molecule along with potential energy distribution (PED) are given in Table-2. The comparative graph between the experimental and calculated IR spectra is displayed in Fig. 2.

TABLE-2
OBSERVED AND CALCULATED FREQUENCIES OF 4FPA USING B3LYP/6-31 + G(d,p) METHOD

Vibrational wavenumber (cm^{-1})			Potential energy distribution (≥ 10%)
Theortical		Experimental	
Unscaled	Scaled	FT-IR	
3626	3488	3649	γNH(100)
3225	3102	3228	γCH(98)
3221	3099	–	γCH(92)
3213	3091	–	γCH(98)
3200	3078	–	γCH(97)
3192	3071	–	γCH(94)
3156	3036	–	γCH(88)
3155	3035	–	γCH(86)
3116	2998	–	γCH(100)
3096	2978	–	γCH(100)
3047	2931	3048	γCH(100)
3036	2921	2523	γCH100)
1720	1655	–	γOC(69) + γCC(11)
1656	1593	–	γCC(41) + βCCC(11)
1645	1582	–	γCC(56) + βCCC(10)
1611	1550	1612	γOC(14) + γCC(44) + βHNC(11)
1545	1486	–	γNC(10) + βHNC(27) + βHCC(10)
1543	1484	–	βHNC(26) + β(17)
1487	1430	–	βHCH(72) + τHCCN(22)
1483	1427	1474	βHCH(80) + τHCCC(15)
1472	1416	–	βHCH(73)
1464	1408	–	βHCH(72) + τHCCN(11)
1447	1392	–	γCC(30)
1428	1374	–	βHCH(68)
1395	1342	–	βHCC(16) + βHCH(11)
1379	1327	1363	βHCC(19) + βHCH(52)
1352	1301	–	γCC(46) + γNC(13)
1324	1274	–	βHCC(12) + βHCC(50)
1299	1250	–	γCC(18) + βHNC(16)

1261	1213	–	γCC(14) + γNC(18) + γFC(20)
1239	1192	1232	γNC(13) + γFC(26) + βHCC(28)
1193	1148	–	γCC(25) + βHCC(22)
1178	1133	–	βHCC(70)
1122	1079	1101	γCC(23) + β (70)
1054	1014	–	βHCH(14) + τHCCN(40)
1043	1003	–	βHCH(12) + τHCCN(50)
1034	995	–	τHCCC(43) + OUT OCCC(19)
1028	989	–	βCCC(85)
1010	972	984	γCC(16) + τHCCC(12)
974	937	–	τHCCC(70) + τCCCC(12)
959	923	–	γCC(34) + τHCCC(23)
950	914	–	τHCCC(71)
888	854	–	γCC(18) + βCCC(17)
865	832	–	τHCCC(32)
840	808	–	τCC(24)
835	803	832	τHCCC(26)
820	789	–	τHCCC(63)
787	757	–	γFC(14) + βCCC(20)
712	685	700	τCCCC(53) + OUT NCCC(10)
663	638	–	γCC(16) + βOCC(10) + βCCC(12) + βNCC(10)
635	611	–	γCC(13) + βCCC(23) + βOCC(14)
606	583	604	τHCCC(26) + OUT OCCC(44)
583	561	–	βOCC(10) + βCCC(14)
553	532	–	OUT CNCC(49)
519	499	–	τCCCC(12) + OUT FCCC(24) + OUT NCCC(16)
476	458	–	βOCC(23) + βNCC(10) + βCCC(14)
431	415	–	βFCC(17) + τCCCC(26)
429	413	–	τ HNCC(20) + τCCCC(30)
417	401	–	βFCC(14) + τ HNCC(64)
381	367	–	βCCN(15) + βCCC(41)
371	357	–	βFCC(26) + OUT FCCC(14) + OUT NCCC(12)
330	317	–	βCCC(47)
295	284	–	βNCC(16) + βCCC(10)
220	212	–	β CNC(11) + βCCC(51)
160	154	–	τCCCN(53)
159	153	–	βCCN(11) + τCCCC(13) + τCCCN(11)
109	105	–	τHCCN(24) + τCCCC(30)
86	83	–	τHCCN(18) + τCCNC(25) + τCCCC(11)
67	64	–	τCCNC(11) + τCCCC (13) + OUT NCCC(21)
61	59	–	τHCCC(53)
39	38	–	τCCNC(29) + τCCCC(36)
30	29	–	β CNC(13) + τCNCC(68)

Carbon-hydrogen (C-H) vibrations: The CH-stretching vibrations of an aromatic compound can be noticed in the range 3100-3000 cm^{-1} [24]. The vibrations are determined at 3102, 3099, 3091, 3078, 3071, 3036, 3035, 2998, 2978, 2931 and 2921 cm^{-1} in the computational spectra, which displays an agreement with the experimental vibrations. The bands appeared inside the experimentally recorded FT-IR spectrum were 3228, 3048 and 2523 cm^{-1}.

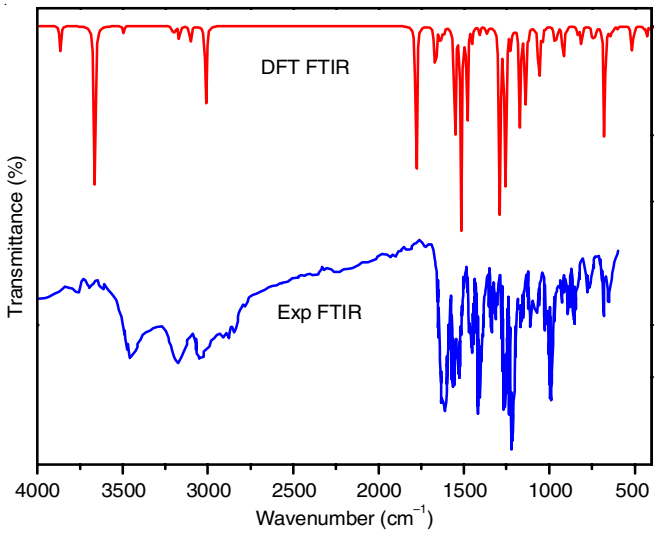

Fig. 2. Experimental and calculated FTIR spectra of 4FPA crystals

C-C ring vibrations: The peaks between 1650 and 1450 cm^{-1} arises generally due to the C–C stretching vibrations [25]. The theoretically calculated carbon-stretching vibrations are located in the range 1593-1250 cm^{-1}. The experimental vibrational bands have also appeared within the range. Few C-C vibrations in ethylenes were shifted to the lower frequency side due to donor of amino group and appeared at 1213, 972, 923, 808, 638, 611 cm^{-1}.

N-H vibrations: The N-H stretching vibrations are generally observed within the range of 3500-3300 cm^{-1}, respectively [26]. The theoretical N-H is 3488 cm^{-1} while the experimental was 3649 cm^{-1}. The disparity in experimental and theoretical results is due to the fact that the gas phase measurements are free from H-bonding interactions which cause comparatively less absorption frequency and large N-H bands to extend in the case of experimental findings.

C-N vibrations: The identifying C-N stretching frequency is difficult due to the overlapping of other vibrations and this vibration is clearly appeared in the region 1386-1266 cm^{-1} [27]. The theoretically scaled wavenumbers are calculated at 1486 and 1192 cm^{-1}.

C=O vibrations: The labeled compound posses carbonyl (C=O) functional group, which commonly seems inside the range of 1740-1680 cm^{-1} [28]. The experimental sharp absorption band observed at 1612 cm^{-1} is stimulated at 1550 cm^{-1}.

C–F vibrations: The vibrations belong to C–F bonds which might be formed among the ring and the halogen atoms are interesting due to the fact the mixing of vibrations is feasible because of the reduced symmetry of the molecules and the presence of heavy atoms [29]. The C–F stretching vibrations appear in the lower range of frequencies and in the present case too, the stretching vibrations were observed at 757 cm^{-1} and the bending vibrations at 415 and 401 cm^{-1}.

Frontier molecular orbitals: The pictograms of the frontier molecular orbitals are shown in Fig. 3. The E_{HOMO}–E_{LUMO} (ΔE_g) of the 4FPA is found to be 4.6373 eV. A large energy gap means high kinetic stability and low chemical reactivity, because it is energetically undesirable to introduce electrons to the

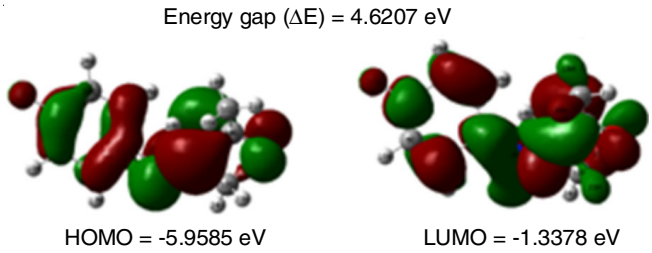

Fig. 3. Frontier molecular pictogram of title compound computed at B3LYP/6-31+G(d,p) level

high-level LUMO and to remove electrons from low-level HOMO [30]. All the parameters are presented in Table-3.

TABLE-3
CALCULATED ENERGY VALUES OF
4FPA BY B3LYP/6-31 + G(d,p) METHOD

Parameters (eV)	B3LYP/6-31 + G(d,p)
E_{HOMO}	-5.9585
E_{LUMO}	-1.3378
Ionization potential (IP)	5.97991
Electron affinity (EA)	1.3426
Energy gap (ΔE)	4.6207
Electronegativity (χ)	3.66125
Chemical potential	-3.66125
Chemical hardness (η)	2.31865
Chemical softness (ζ)	0.21564
Electrophilicity index (ψ)	2.89063

Molecular electrostatic potential surface (MEP): In Fig. 4a, the red represents electron concentric areas while the blue is the opposite. The red colour near O_2 indicates oxygen is more electrophilic attack in carboxyl group. The blue region around N3-H15 indicates the maximum electrostatic potential of the amino group. In addition, the MEP contour plot is a 2D display where the values of the relative electron density lie within a specific range (-6.111×10^{-2} to $+ 6.111 \times 10^{-2}$). But this MEP surface has been drawn for a selected iso-surface value. In order to see the entire MEP surfaces, we plot each surface as a contour around the molecule. In Fig. 4b, each contour curves around the molecule is the MEP surface; the outer contour is with lower iso-surface value while the inner contour is with higher iso-surface value.

Reactive site analysis through Fukui function: The average local ionization energy at the molecular surface is an effective parameter for defining reactive sites [31]. This approach is already used where MEPs of molecules are discussed. On the other hand, Fukui function analysis can give clearer overview of the nucleophilic, electrophilic and radial attack regions of the molecules using the anion and cation forms of the molecules as well as their neutral form. The Fukui function [32] is define as follow:

$$f(\vec{r}) = \left(\frac{\partial \rho(\vec{r})}{\partial N}\right)_v \quad (1)$$

where v (constant) in the partial derivative is external potential, N is number of electrons of the system. The anion, neutral and cation forms of the molecules were identified based on electron density as (N+1), (N) and (N-1), respectively. To calculate nucleophilic and electrophilic attack regions, the equations are as follows;

Nucleophilic attack:

$$f^{+}(\vec{r}) = \rho_{N+1}(\vec{r}) - \rho_{N}(\vec{r}) \quad (2)$$

Electrophilic attack:

$$f^{-}(\vec{r}) = \rho_{N}(\vec{r}) - \rho_{N-1}(\vec{r}) \quad (3)$$

Radial attack:

$$f^{0}(\vec{r}) = \frac{\left[f^{+}(\vec{r})/f^{-}(\vec{r})\right]}{2} \quad (4)$$

The dual descriptor is determined as $\Delta f(\vec{r}) = f^{+}(\vec{r}) - f^{-}(\vec{r})$ the difference in nucleophilic and electrophilic characters, which is a simultaneous presentation of both effects. Also, to the differences in the spin density of cation and anion form the followed equation show, named dual descriptor:

Dual descriptor from spin states:

$$\Delta f(\vec{r}) = \rho^{s}_{N+1}(\vec{r}) - \rho^{s}_{N-1}(\vec{r}) \quad (5)$$

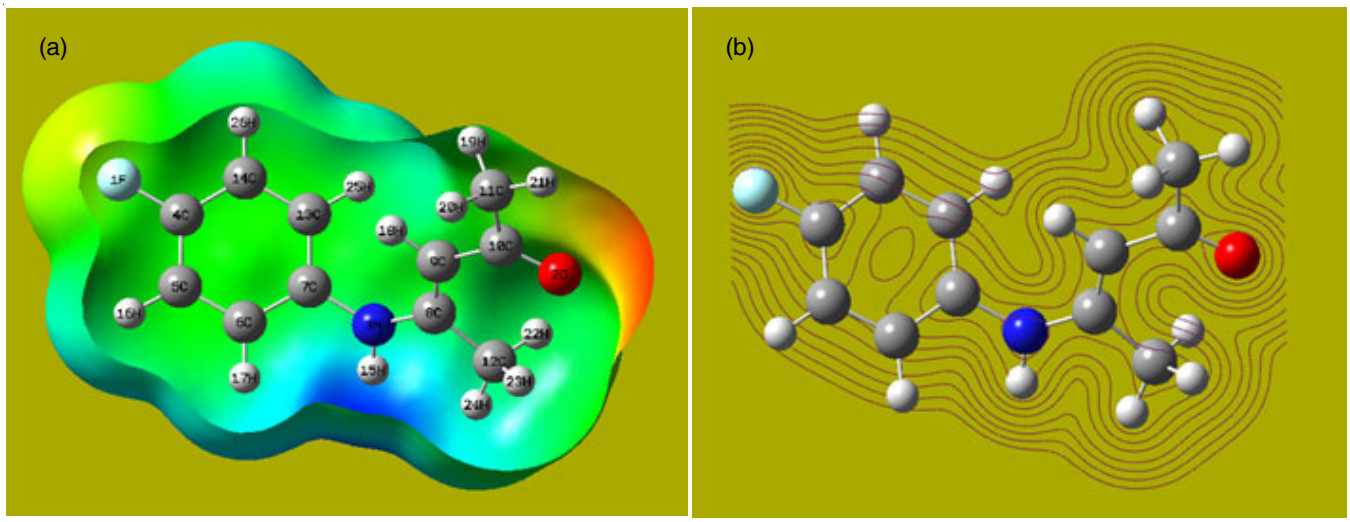

Fig. 4. MEP and electrostatic contour map of 4FPA crystals

The $\Delta f(\vec{r})$ is values of electrophilic or nucleophilic regions in a title molecule, as negative or positive, respectively. The isosurface value of visualized surfaces are taken as 0.4, for $f^{+}(\vec{r})$, $f^{-}(\vec{r})$ and $\Delta f(\vec{r})$, respectively. The surfaces of these three forms are given as Fig. 5, the negative region is defined in the purple region, while the positive region is seen as green. The calculated charges for neutral, anion and cation, condensed dual descriptor values are listed in Table-4.

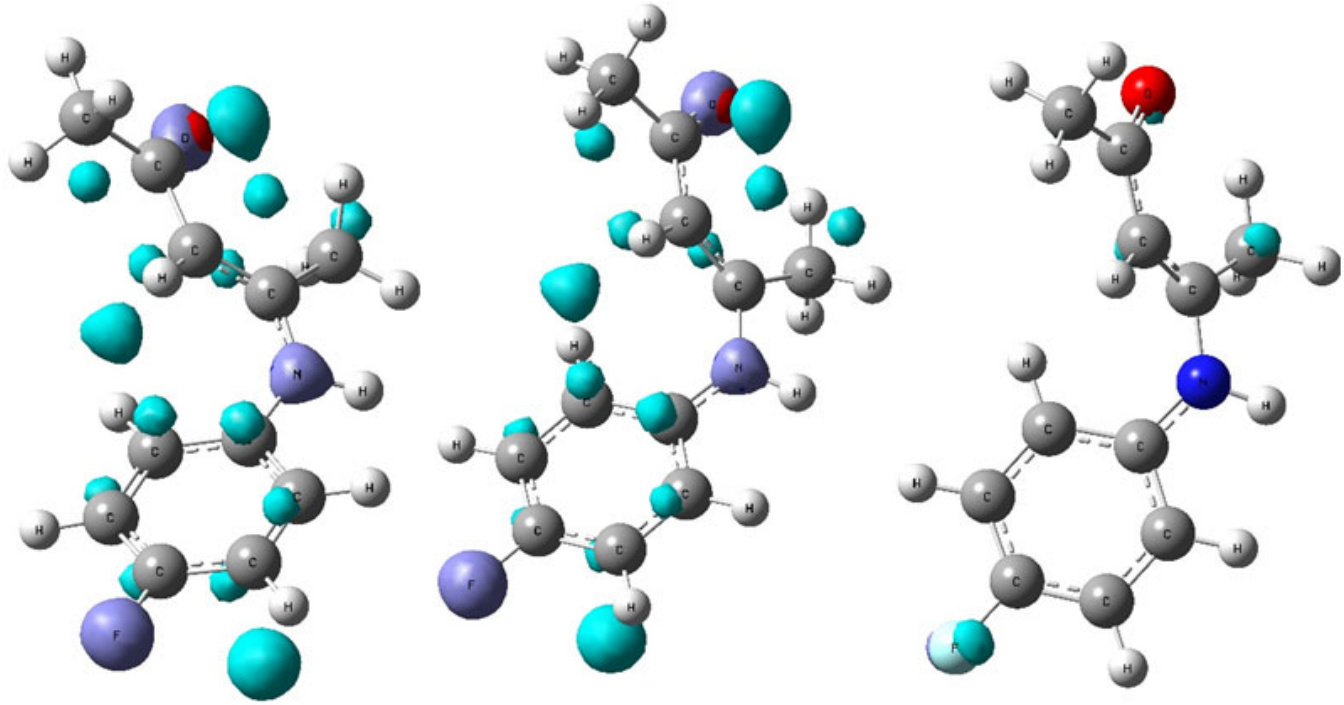

Fig. 5. Isosurface of Fukui functions and dual descriptor of 4FPA molecule

TABLE-4
ELECTRON DENSITY VALUES ANION (N + 1), NEUTRAL (N) AND CATION (N-1) FORMS, ATTACK REGIONS AND DUAL DESCRIPTOR OF 4FPA

Atom	Label	Neutral	Anion	Cation	Electrophilic attack	Nucleophilic attack	Radical attack	Dual descriptor
1	F	-0.116	-0.164	-0.053	0.063	0.047	0.055	-0.016
2	O	-0.288	-0.407	-0.197	0.091	0.119	0.105	0.029
3	N	-0.072	-0.093	0.025	0.097	0.021	0.059	-0.076
4	C	0.092	0.041	0.152	0.059	0.052	0.055	-0.007
5	C	-0.047	-0.079	-0.008	0.039	0.032	0.035	-0.007
6	C	-0.044	-0.083	-0.006	0.038	0.039	0.038	0.001
7	C	0.043	0.037	0.068	0.025	0.006	0.015	-0.020
8	C	0.085	-0.009	0.119	0.034	0.094	0.064	0.060
9	C	-0.120	-0.144	0.004	0.124	0.024	0.074	-0.099
10	C	0.134	0.045	0.168	0.034	0.089	0.061	0.055
11	C	-0.093	-0.119	-0.074	0.019	0.026	0.022	0.007
12	C	-0.081	-0.113	-0.065	0.016	0.032	0.024	0.016
13	C	-0.035	-0.070	-0.007	0.028	0.036	0.032	0.008
14	C	-0.045	-0.069	-0.012	0.033	0.024	0.028	-0.009
15	H	0.123	0.085	0.161	0.039	0.037	0.038	-0.002
16	H	0.056	0.030	0.085	0.029	0.026	0.027	-0.003
17	H	0.046	0.015	0.071	0.026	0.030	0.028	0.005
18	H	0.022	-0.003	0.055	0.033	0.025	0.029	-0.008
19	H	0.037	0.007	0.056	0.020	0.029	0.025	0.009
20	H	0.038	0.005	0.058	0.020	0.033	0.026	0.012
21	H	0.038	0.007	0.065	0.027	0.030	0.029	0.004
22	H	0.049	0.004	0.072	0.023	0.045	0.034	0.022
23	H	0.045	0.021	0.064	0.019	0.024	0.022	0.004
24	H	0.030	-0.008	0.053	0.023	0.037	0.030	0.014
25	H	0.050	0.029	0.064	0.015	0.020	0.018	0.006
26	H	0.056	0.035	0.083	0.027	0.021	0.024	-0.006

Thermodynamic properties: Thermodynamic properties of 4FPA molecule are of critical importance for the chemical industry and technologies. The changes of the heat capacity (C), entropy (S) and enthalpy (H) depend on temperature can give an idea about the phase transition and decomposition properties of chemical substances. A vibration analysis based on theoretical harmonic frequencies was performed to see the effect of temperature on properties from 100 to 1000 K, for the 4FPA molecule. The results are collected and graphed in Fig. 6. The relationship between temperature and thermodynamic properties is expressed by the following quadratic formulas derived from empirical approaches.

$$C = 3.54412 + 0.185172T - 7.6464 \times 10^{-5}T^2 \quad (R^2 = 0.9995) \quad (6)$$

$$S = 62.12912 + 0.212488T - 5.1907 \times 10^{-5}T^2 \quad (R^2 = 0.9999) \quad (7)$$

$$\Delta H = -2.189195 + 0.02520T + 5.0660 \times 10^{-5}T^2 \quad (R^2 = 0.9996) \quad (8)$$

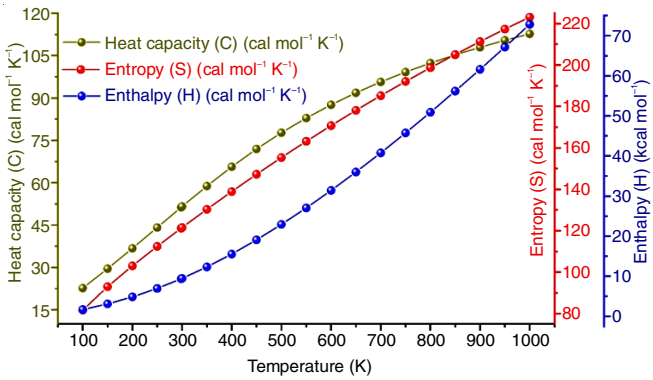

Fig. 6. The correlation graphics of heat capacity, entropy, enthalpy and temperature of 4FPA molecule

The quadratic formulas are simply experimental and represent possible contributions from normal modes of translation, rotation and vibration. In fact, the temperature dependence of each function, the vibrational in properties, is more complex. Also, vibration frequencies were calculated within the harmonic approximation and any possible handicapped rotation of the NH group was ignored. These approaches lead to non-zero values for enthalpy and heat capacity at absolute zero.

Non-covalent interactions: Non-covalent interactions such as hydrogen bonding, van der Walls interactions and steric effects can be analyzed by reduced density gradient (RDG) analysis, an effective method described by Johnson *et al.* [33] as follows:

$$RDG(r) = \frac{1}{2(3\pi^2)^{1/3}} \frac{|\nabla\rho(r)|}{\rho(r)^{4/3}} \quad (9)$$

Analysis of inter- and intra-molecular interactions in real space, depending on electron density and derivatives, is easily done with this approach. The RDG and colour scaled visualization of intramolecular interactions, which are produced by using Multiwfn [20] and VMD programs [21], for the 4FPA molecule given in Fig. 7.

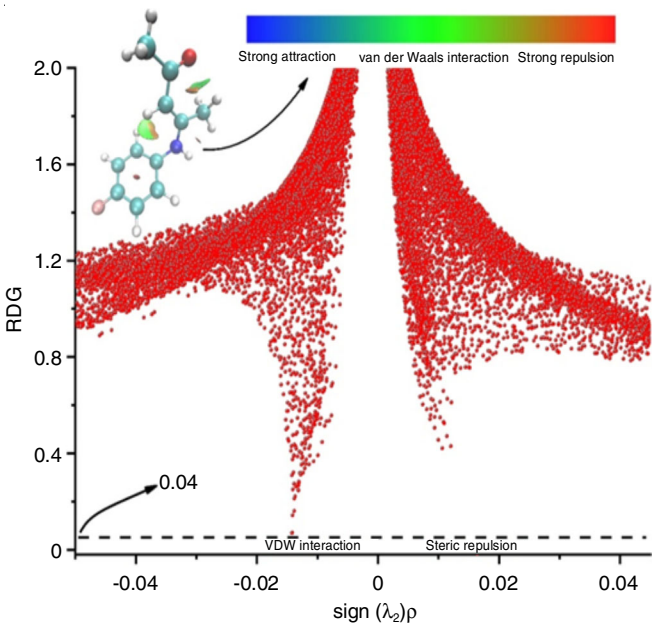

Fig. 7. The reduced density gradient (RDG) of 4FPA molecules

The reduced density gradient (RDG) *versus* electron density (ρ) multiplied by the sign of λ_2 is used to investigate and visualize a wide variety of the interaction types. The sign of λ_2 is a criterion for classifying as a bonding ($\lambda_2 < 0$), non-bonding ($\lambda_2 > 0$) interactions and very weak interactions in the region close to zero. The spike near zero indicative of very weak interaction in the system for studied molecule, located around -0.015 of sign $(\lambda_2)\rho$ and identified as van der Waals (VDW) interactions. The RDG values near 0.02 indicate the non-bonding interaction of strong repul-sion or steric effect of the ring.

Non-linear optical properties: In this study, dipole moment, polarizability and the first-order hyperpolarizability of 4FPA molecule along with related properties (μ, α and β) were calculated by using DFT/B3LYP method with 6-31+G (d,p) basis set. The data of the non-linear optical properties are listed in Table-5. Theoretically, the first hyperpolarizability of 4FPA molecule is 15.5 times greater than that of urea. Therefore, investigated molecule will show a more non-linear optical response and might be used as non-linear optical (NLO) material.

TABLE-5
NON-LINEAR OPTICAL PROPERTIES OF 4FPA MOLECULES

Parameters	B3LYP/6-31+G(d,p)	Parameters	B3LYP/6-31+G(d,p)
μ_x	2.8916	β_{xxx}	48.8
μ_y	-1.9459	β_{xxy}	-33.8
μ_z	-0.2524	β_{xyy}	-61.62
μ(D)	3.4945	β_{yyy}	462.64
α_{xx}	147.66	β_{zxx}	-33.23
α_{xy}	-32.37	β_{xyz}	-76.91
α_{yy}	157.11	β_{zyy}	294.28
α_{xz}	-2.51	β_{xzz}	-22.25
α_{yz}	41.82	β_{yzz}	163.1
α_{zz}	144.9	β_{zzz}	51.67
α_0 (e.s.u)	2.2213×10^{-23}	β_{tot} (e.s.u)	5.791×10^{-30}
α (e.s.u)	7.84219×10^{-23}		

Conclusion

The (*Z*)-4-((4-fluorophenyl)amino)pent-3-en-2-one (4FPA) single crystal was grown using a slow evaporation solution growth technique. Single crystal XRD study revealed that 4FPA crystal was crystallized in a triclinic system with a space group of *P*1. The experimental FT-IR results of 4FPA were also found in agreement with the DFT vibrational data. The 2D fingerprint analysis revealed that the interactions between H···H and C···H are more dominant in the 4FPA compound. The photophysical property was evaluated by UV-vis *via* frontiers molecular orbitals. The NBO analysis has provided the insight into the type of hybridization and the nature of bonding in title compound. The strongest electron donation occurs from a lone pair to the anti-bonding acceptor LP(1) N3 to π*(C8-C9). According to the MEP diagrams, the oxygen atom on the compound is rich in electrons resulted in the nucleophilic attack site of this molecule. Reactive nature of 4FPA was explored by Fukui function analysis from both surface mapping of nucleophilic/electrophilic regions and the dual descriptor values were calculated according to Hirshfeld population analysis. The non-covalent interactions of title molecule were located around -0.015 of sign $(\lambda_2)\rho$ identified as van der Waals interactions, on the H-atom on the ring and with the methyl group. Theoretically, the first hyperpolarizability of 4FPA is 15.5 times greater than that of urea. Therefore, investigated molecule might be used as non-linear optical (NLO) material.

CONFLICT OF INTEREST

The authors declare that there is no conflict of interests regarding the publication of this article.

REFERENCES

1. C.M. Kascheres, *J. Braz. Chem. Soc.*, **14**, 945 (2003); https://doi.org/10.1590/S0103-50532003000600012
2. S.K. Maury, S. Kumari, A. Kamal, H.K. Singh, D. Kumar and S. Singh, *Tetrahedron Lett.*, **61**, 152383 (2020); https://doi.org/10.1016/j.tetlet.2020.152383
3. M.A. Bhat, M.A. Al-Omar, A.M. Naglah and A.A. Khan, *J. Chem.*, **2019**, Article ID 2467970 (2019); https://doi.org/10.1155/2019/2467970
4. R. Kumar, N. Saha, P. Purohit, S.K. Garg, K. Seth, V.S. Meena, S. Dubey, K. Dave, R. Goyal, S.S. Sharma, U.C. Banerjee and A.K. Chakraborti, *Eur. J. Med. Chem.*, **182**, 111601 (2019); https://doi.org/10.1016/j.ejmech.2019.111601
5. J. Apraku and C.O. Okoro, *Bioorg. Med. Chem.*, **27**, 161 (2019); https://doi.org/10.1016/j.bmc.2018.11.033
6. M.M. Ghorab, F.A. Ragab, H.I. Heiba, M.G. El-Gazzar and M.G.M. El-Gazzar, *Bioorg. Med. Chem. Lett.*, **28**, 1464 (2018); https://doi.org/10.1016/j.bmcl.2018.03.089
7. N.D. Eddington, D.S. Cox, R.R. Roberts, J.P. Stables, C.B. Powell and K.R. Scott, *Curr. Med. Chem.*, **7**, 417 (2000); https://doi.org/10.2174/0929867003375092
8. H.M. Gaber, Z.A. Muhammad, S.M. Gomha, T.A. Farghaly and M.C. Bagley, *Curr. Organ. Chem.*, **21**, 2168 (2017); https://doi.org/10.2174/1385272821666170523115019
9. A.S. Shawali, *J. Adv. Res.*, **1**, 225 (2010); https://doi.org/10.1016/j.jare.2010.07.002
10. L.B.A. Oliveira, L.A. Júnior and G. Colherinhas, *New J. Chem.*, **42**, 12032 (2018); https://doi.org/10.1039/C8NJ01842A
11. D.F.S. Machado, T.O. Lopes, I.T. Lima, D.A. da Silva Filho and H.C.B. de Oliveira, *J. Phys. Chem. C*, **120**, 17660 (2016); https://doi.org/10.1021/acs.jpcc.6b01567
12. R. Huma, T. Mahmud, N. Idrees, M.J. Saif, R. Munir and N. Akbar, *J. Chem. Crystallogr.*, **50**, 187 (2020); https://doi.org/10.1007/s10870-019-00786-5
13. S.I. Vdovenko, I.I. Gerus, Y.I. Zhuk, V.P. Kukhar, M. Pagacz-Kostrzewa, M. Wierzejewska and C.-G. Daniliuc, *J. Mol. Struct.*, **1128**, 741 (2017); https://doi.org/10.1016/j.molstruc.2016.09.049
14. M. Saghi and A. Arastehnodeh, *Int. J. New Chem.*, **5**, 65 (2018); https://doi.org/10.22034/IJNC.2018.32806
15. R. Dobosz, R. Gawinecki and B. Osmialowski, *Struct. Chem.*, **21**, 1283 (2010); https://doi.org/10.1007/s11224-010-9674-y
16. M. Stojanovic, S. Bugarski and M. Baranac-Stojanovic, *J. Org. Chem.*, **85**, 13495 (2020); https://doi.org/10.1021/acs.joc.0c01537
17. Y.N. Mabkhot, A. Barakat, S.M. Soliman, T.T. El-Idreesy, H.A. Ghabbour and S.S. Al-Showiman, *J. Mol. Struct.*, **1130**, 62 (2017); https://doi.org/10.1016/j.molstruc.2016.10.001
18. M.J. Frisch, G.W. Trucks, H.B. Schlegel, G.E. Scuseria, M.A. Robb, J.R. Cheeseman, G. Scalmani, V. Barone, B. Mennucci, G.A. Petersson, H. Nakatsuji, M. Caricato, X. Li, H.P. Hratchian, A.F. Izmaylov, J. Bloino, G. Zheng, J.L. Sonnenberg, M. Hada, M. Ehara, K. Toyota, R. Fukuda, J. Hasegawa, M. Ishida, T. Nakajima, Y. Honda, O. Kitao, H. Nakai, T. Vreven, J.A. Montgomery Jr., J.E. Peralta, F. Ogliaro, M. Bearpark, J.J. Heyd, E. Brothers, K.N. Kudin, V.N. Staroverov, R. Kobayashi, J. Normand, K. Raghavachari, A. Rendell, J.C. Burant, S.S. Iyengar, J. Tomasi, M. Cossi, N. Rega, J.M. Millam, M. Klene, J.E. Knox, J.B. Cross, V. Bakken, C. Adamo, J. Jaramillo, R. Gomperts, R.E. Stratmann, O. Yazyev, A.J. Austin, R. Cammi, C. Pomelli, J.W. Ochterski, R.L. Martin, K. Morokuma, V.G. Zakrzewski, G.A. Voth, P. Salvador, J.J. Dannenberg, S. Dapprich, A.D. Daniels, Ö. Farkas, J.B. Foresman, J.V. Ortiz, J. Cioslowski and D.J. Fox, Gaussian 09 Revision D. 01 (2009).
19. M.H. Jamroz, *Spectrochim. Acta A Mol. Biomol. Spectrosc.*, **114**, 220 (2013); https://doi.org/10.1016/j.saa.2013.05.096
20. T. Lu and F. Chen, *J. Comput. Chem.*, **33**, 580 (2012); https://doi.org/10.1002/jcc.22885
21. W. Humphrey, A. Dalke and K. Schulten, *J. Mol. Graph.*, **14**, 33 (1996); https://doi.org/10.1016/0263-7855(96)00018-5
22. K. Fukui, *Science*, **218**, 747 (1982); https://doi.org/10.1126/science.218.4574.747
23. P. Divya, P. Muthuraja, M. Dhandapani and V. Bena, *Chem. Phys. Lett.*, **706**, 295 (2018); https://doi.org/10.1016/j.cplett.2018.06.021
24. N. Swarnalatha, S. Gunasekaran, S. Muthu and M. Nagarajan, *Spectrochim. Acta A Mol. Biomol. Spectrosc.*, **137**, 721 (2015); https://doi.org/10.1016/j.saa.2014.08.125
25. K.R. Santhy, M.D. Sweetlin, S. Muthu, M. Raja and C.S. Abraham, *Optik*, **182**, 1211 (2019); https://doi.org/10.1016/j.ijleo.2019.02.010
26. R.M. Silverstein and G.C. Bassler, Spectrometric Identification of Organic Compounds, Wiley: NewYork (1963).
27. M. Silverstein, G.C. Basseler and C. Morill, Spectrometric Identification of Organic Compounds, Wiley: NewYork (1981).
28. M.U. Kumar, A.P. Jeyakumari, M. Suresh, S. Chandran and G. Vinitha, *Mater. Res. Express*, **6**, 75102 (2019); https://doi.org/10.1088/2053-1591/ab13c7
29. S. Parveen S, M.A. Al-Alshaikh, C.Y. Panicker, A.A. El-Emam, B. Narayana, V.V. Saliyan, B.K. Sarojini and C. Van Alsenoy, *J. Mol. Struct.*, **1112**, 136 (2016); https://doi.org/10.1016/j.molstruc.2016.02.018
30. Z. Gültekin, Z. Demircioglu, W. Frey and O. Büyükgüngör, *J. Mol. Struct.*, **1199**, 126970 (2020); https://doi.org/10.1016/j.molstruc.2019.126970
31. P. Sjoberg, J.S. Murray, T. Brinck and P. Politzer, *Can. J. Chem.*, **68**, 1440 (1990); https://doi.org/10.1139/v90-220
32. P. Fuentealba, E. Florez and W. Tiznado, *J. Chem. Theory Comput.*, **6**, 1470 (2010); https://doi.org/10.1021/ct100022w
33. E.R. Johnson, S. Keinan, P. Mori Sánchez, J. Contreras García, A.J. Cohen and W. Yang, *J. Am. Chem. Soc.*, **132**, 6498 (2010); https://doi.org/10.1021/ja100936w